# Three Different Tyrosyl Radicals Identified in l-Tyrosine HCl Crystals upon γ-Irradiation: Magnetic Characterization and Temporal Evolution

**ARTICLE** *in* THE JOURNAL OF PHYSICAL CHEMISTRY B · APRIL 2008

Impact Factor: 3.3 · DOI: 10.1021/jp710220u · Source: PubMed



**5 AUTHORS**, INCLUDING:

Vasile Chis
Babeş-Bolyai University
**109** PUBLICATIONS **719** CITATIONS
SEE PROFILE

Alfonso Zoleo
University of Padova
**35** PUBLICATIONS **259** CITATIONS
SEE PROFILE

Alberto Mezzetti
University of Lille Nord de France
**47** PUBLICATIONS **365** CITATIONS
SEE PROFILE

# Three Different Tyrosyl Radicals Identified in L-Tyrosine HCl Crystals upon γ-Irradiation: Magnetic Characterization and Temporal Evolution

**Anna Lisa Maniero,*,† Vasile Chis,‡ Alfonso Zoleo,† Marina Brustolon,† and Alberto Mezzetti§**

*Università degli Studi di Padova, Dipartimento di Scienze Chimiche, Via Marzolo 1, I-35131 Padova, Italy, Babeş-Bolyai University, Faculty of Physics, 1 Kogălniceanu, RO-400084 Cluj-Napoca, Romania, and Laboratoire de Spectrochimie Infrarouge et Raman, UMR CNRS 8516, Université de Sciences et Technologies de Lille, Bat C5, Cité Scientifique, 59655 Villeneuve d'Ascq, France*

*Received: October 22, 2007; In Final Form: December 17, 2007*

High-frequency electron paramagnetic resonance (EPR) and X-band electron−nuclear double resonance (ENDOR) spectroscopies were used to investigate the effect of γ-irradiation on single crystals of L-tyrosine hydrochloride at room temperature. The oxidation product is the tyrosyl radical formed by hydrogen abstraction from the phenolic group; interestingly, on freshly irradiated crystals, two tyrosyl radicals were identified, characterized by slightly different magnetic parameters. In particular, one of the two radicals, with a $g_{xx}$ value of 2.00621, has its phenoxyl oxygen strongly hydrogen-bonded to one or more donors; to our knowledge, this is the lower $g_{xx}$ value reported for tyrosyl radicals. These two oxidation radicals are found to evolve very slowly to a third, single more stable radical conformation. To interpret the experimental data, a possible molecular scenario is presented, where the process of radical formation can be seen as a hydrogen atom transfer or a proton-coupled electron transfer. These processes seem to be controlled by the specific network of hydrogen-bond interactions present in the crystal. The results are discussed in relation to their relevance for the interpretation of EPR spectra of tyrosyl radicals in biological systems.

## Introduction

Amino-acid radicals are important intermediates in a large variety of biochemical processes.[1−4] In particular, tyrosine is involved in many protein redox processes, being one of the most easily oxidizable amino acids. Tyrosyl radicals directly participate in the enzyme activity of ribonucleotide reductase,[5] prostaglandin-H synthase[6] and the water-splitting enzyme in plant photosynthesis.[7] Tyrosyl radicals have also been identified as intermediates or as a part of the electron transfer chain of several other enzymes.[8−14] Several recent reviews are entirely focused on the enzymatic role of the tyrosyl radical.[15−18] A growing number of studies are also pointing out a possible key role of tyrosyl radicals in several diseases, including atherosclerosis,[19,20] Alzheimer disease[21,22] and other neurological disorders.[23]

The technique of choice to investigate the properties and role of radicals in biological systems is electron paramagnetic resonance (EPR) spectroscopy, because of its selectivity and of the wealth of structural and dynamic information it can provide.[24] Indeed, almost all of the above-mentioned works were carried out using EPR spectroscopy as the key technique. These studies on tyrosyl radicals in biological systems have also prompted a series of parallel EPR investigations on tyrosyl and phenoxyl radicals in model systems, as phenol-based model compounds,[25,26] small peptides (ref 27 and references therein), especially engineered proteins,[28] and in different media, like γ-irradiated single crystals,[29−33] aqueous solutions[34−36] and glassy matrices (refs 37−39 and references therein). Several theoretical calculations have also been carried out (refs 40−44 and references therein) in order to rationalize the relationship between the magnetic properties and the underlying molecular structure and dynamics.

Characteristic EPR parameters such as $g$ and hyperfine coupling (hfc) tensors can provide precise information on the electronic and molecular structure of the tyrosyl radical and on its surroundings. In particular, the $g$ tensor depends both on the electronic structure of the radical and on the radical environment.[44] A direct correlation has been found between one of the principal values of the tensor, the $g_{xx}$ value (corresponding to the direction parallel to the radical C−O bond) and the presence of a hydrogen bond involving the tyrosyl oxygen as the acceptor (tyrO$^{\bullet}$···H−D).[40,44] This has pointed out the possibility of using the $g_{xx}$ value as a probe to assess the H-bonding state of the phenoxyl oxygen. This is of particular relevance because the H-bonding state of the phenoxyl oxygen can play a crucial role in the redox behavior of tyrosyl radical in biological systems.[15,18] Hfc tensors are other important EPR parameters, providing information on the spin density map of the radical and, in the case of β protons, on the methylene dihedral angle.[45] Several studies have suggested that the strength of a tyrO$^{\bullet}$···H−D interaction modulates the spin density of the radical.[25,40,46]

In a previous paper, we have presented a detailed investigation of the tyrosyl radical produced by γ-ray irradiation in single crystals of *N*-acetyl-L-tyrosine.[31] In general, the use of an oriented sample greatly enhances the information we can obtain from EPR spectroscopy, as the comparison with the crystallographic data allows the precise assignment of the hfc and $g$ tensor elements. Furthermore, in the case of *N*-acetyl-L-tyrosine, the phenoxyl oxygen of the tyrosyl radical is not involved in H-bond interactions;[47] therefore, its $g_{xx}$ value represents a

* Corresponding author. E-mail: annalisa.maniero@unipd.it. Phone: +39 049 8275109. Fax: +39 049 8275239.
† Università degli Studi di Padova.
‡ Babeş-Bolyai University.
§ Université de Sciences et Technologies de Lille.

10.1021/jp710220u CCC: $40.75 
Published on Web 03/05/2008

reference model for biological tyrosyl radical with a "free" phenoxyl oxygen.

The aim of the present work is the investigation of a tyrosyl radical with its phenoxyl oxygen involved in a H-bond interaction as an acceptor, in an ordered system: we have studied the tyrosyl radical formed by $\gamma$-ray irradiation in single crystals of L-tyrosine hydrochloride (L-Tyr HCl). In the undamaged crystal, the oxygen of the tyrosine phenolic group is involved in a H-bond interaction with the OH of the COOH moiety.[48] The tyrosyl radical retains this H-bond interaction, as it occupies the same position as the undamaged molecule in the crystal lattice.[30] For this reason, this system is considered the reference model for tyrosyl radicals involved in a H-bond interaction.

The $\gamma$-irradiated L-Tyr HCl crystals have been already investigated by X-band cw-EPR.[30,32,33] An electron−nuclear double resonance (ENDOR) study at 4 K was performed on crystals X-irradiated at the same temperature.[29] High-frequency EPR spectra have been reported for finely grinded L-Tyr HCl crystals.[14] However, in all of the above-mentioned systems, the characterization of the tyrosyl radical remained somehow incomplete. For a more complete characterization, in this paper, we have used an integrated approach which combines ENDOR spectroscopy on single crystals and high-frequency EPR experiments on powders. The use of both techniques has allowed us to disentangle spectral contributions arising from different radicals and to obtain precise measurements of the tensors' elements. Moreover, the HF-EPR spectra were recorded at different times after the irradiation and this has allowed us to follow the evolution with time of the initially formed radicals.

The present investigation interestingly shows that $\gamma$-irradiation at room temperature induces the formation of two different tyrosyl radicals, almost identical in structure and lattice position but characterized by slightly different $g$ and hfc tensors. We explain this fact by assuming that the two radicals are involved in different H-bond (tyrO$^{\bullet}\cdots$H−D) interactions. These radicals are found to slowly evolve toward a third, more stable form. Quantum mechanical calculations have allowed us to propose a detailed molecular scenario for the formation and time evolution of the radicals.

## Experimental Methods

**Sample Preparation.** Single crystals of L-Tyr HCl were grown at room temperature by slow evaporation of a saturated solution of L-tyrosine in concentrated HCl. The dimensions of the crystals were about $2 \times 2 \times 4$ mm$^3$. The crystals were irradiated at room temperature by $\gamma$-rays from a $^{60}$Co source with a dose of 6 MRad.

The crystal structure from both X-ray diffraction methods[49] and neutron diffraction methods[48] is available in the literature. L-Tyr HCl crystallizes in the monoclinic space group $P2_1$, with cell parameters $a = 11.083$ Å, $b = 9.041$ Å, $c = 5.099$ Å, and $\beta = 91.82°$ and two molecules per unit cell.

Since L-Tyr HCl is hygroscopic, the samples were kept in a sealed container to prevent damage.

**X-Band EPR and ENDOR Measurements.** X-band EPR and ENDOR spectra were recorded at a frequency of 9.4 GHz using a conventional Bruker ER200D spectrometer interfaced with a Bruker data system ESP1600 and equipped with a Bruker variable temperature unit. The radio frequency (RF) was generated by a Rhode & Schwartz SMX synthesizer and frequency-modulated at 25 kHz by using an EG & G 5208 lock-in; the ENDOR signal was recorded as the first derivative. Amplification of the RF is achieved with an ENI A-300 amplifier. The single-crystal spectra were recorded at a temperature of 150 K by rotating the crystal around the three crystallographic axes $a$, $b$ and $c^*$; the spectra were taken every 6°. The ENDOR spectra were recorded only on freshly irradiated crystals, within 1 month from the irradiation.

**High-Frequency EPR Measurements.** High-frequency EPR (HF-EPR) spectra (at about 220 and 330 GHz) of powder samples were obtained at the NHMFL in Tallahassee (FL) with a homemade spectrometer.[50] The spectrometer was used in its basic configuration ("single pass" transmission mode). The spectra were obtained modulating the magnetic field at a frequency of 8 kHz with a modulation amplitude of 0.01−0.07 mT; the temperature was in the range 30−280 K depending on the sample and on the microwave frequency. For $g$ factor measurements, either DPPH (Sigma, ground to a fine powder) or a polycrystalline sample of manganese oxide diluted in calcium oxide was used as the internal standard to calibrate the magnetic field. The use of manganese oxide allows also calibrating the field linearity of the sweeping coil employed in high-resolution experiments.[50] All of the powdered samples were pressed in pellets to avoid possible orientation in the magnetic field. The HF-EPR spectra were recorded on freshly irradiated finely ground crystals, and on finely ground aged crystals (about 1 year old).

**Computational Details.** Calculations were performed with the software package Gaussian 03.[51] Geometry optimizations were carried out with the semiempirical PM3 method,[52] while calculations of magnetic properties were done by DFT methods with the exchange correlation functional B3LYP[53,54] and the basis set 6-31+G(d,p).[55] The GIAO method was used for calculating $g$ tensors.[56]

We performed PM3 calculations on the extended molecular system shown in Figure 1a, both with and without the HCl molecule. These two systems represent a simple model for two possible environments that, in our scenario, the tyrosyl radicals might experience in the irradiated crystals (see the Discussion). The arrangement consists of a tyrosyl radical, R, H-bonded to a tyrosine molecule, M, (through the carboxyl group of M) and, if present, to a HCl molecule, which in turn interacts, through hydrogen bonds, with three nearby amines. With respect to the crystal structure, in our model system, we replaced the protonated amino groups of M and R, and their chloride counterions, with neutral aminic groups. Similarly, the three neutral amines A, B and C binding HCl (see Figure 1a) replaced the three protonated amino groups of tyrosine molecules, with their respective chlorides. Apart from these differences, in the starting geometry, the considered atoms were in the same position as in the crystal lattice. From this arrangement, both with and without HCl, we optimized at the PM3 level the coordinates of the phenoxyl ring atoms, the M carboxyl hydrogen and, when present, the HCl, freezing all of the other atoms to their crystallographic positions (Figure 1a represents the obtained PM3 optimized geometry). We simplified the two optimized arrangements (with and without HCl), removing the three amines A, B and C and part of the molecule M, as in Figure 1b, to perform DFT calculations of the $g$ tensors.

## Results

**X-Band cw-EPR.** Due to the monoclinic structure of L-Tyr HCl, two magnetically nonequivalent sites are present. Therefore, at any orientation of the crystal in the magnetic field, the spectrum is given by the superposition of the spectra due to radicals in the two crystal sites. However, the two sites become magnetically equivalent when the magnetic field is along a crystallographic axis or in the $ac^*$ crystallographic plane.

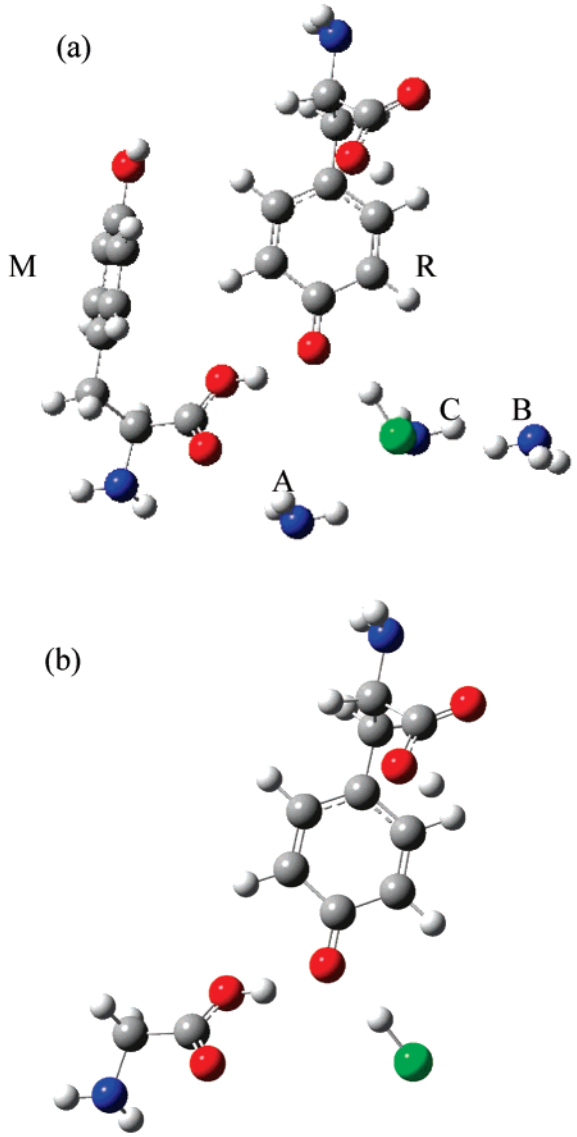


**Figure 1.** (a) Molecular system used in the PM3 calculations (green = chlorine, blue = nitrogen, red = oxygen, white = hydrogen). (b) Simplified molecular system used in the DFT calculations (see text).

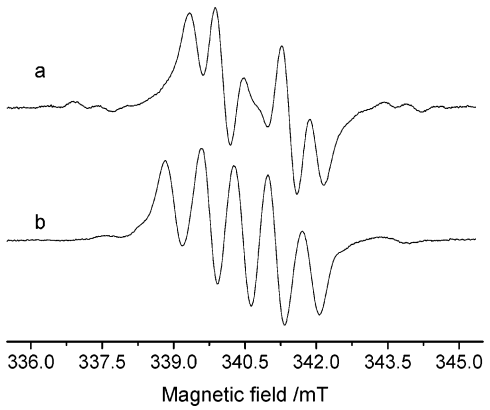


**Figure 2.** X-band cw-EPR spectra recorded with the magnetic field along the crystallographic axis *b* (trace a) and with the magnetic field in the *ab* plane at 30° from axis *a* (trace b).

The X-band cw-EPR spectra for two different orientations of the magnetic field are reported in Figure 2 (Figure 2a, magnetic field along the crystal axis *b*; Figure 2b, magnetic field in the *ab* plane at 30° from the axis *a*). The dominant feature of the spectra is a central multiplet spread over about 30 G, which can be interpreted as a doublet of triplets 1:2:1, due to the interaction of the unpaired electron with three protons, two of them almost equivalent. This main spectral pattern varies little with the orientation of the crystal in the magnetic field. On the basis of the comparison with the results obtained previously on $\gamma$-irradiated L-Tyr HCl single crystals[29,30,32] as well as on $\gamma$- irradiated *N*-acetyl-L-tyrosine single crystals,[31] we identified the main free radical with the tyrosyl radical formed by loss of the hydrogen atom from the OH phenolic group (shown in Figure 3).

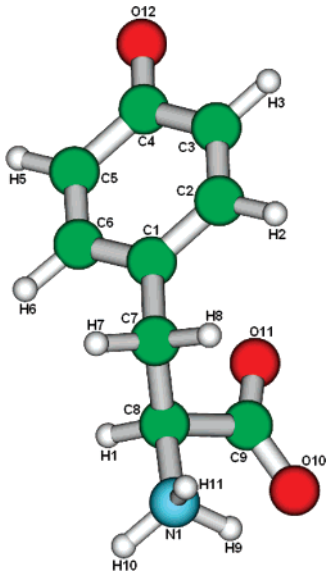


**Figure 3.** Atom numbering scheme for the tyrosyl radical.

The spectra also show weaker resonances evident at the sides of the basic multiplet. These signals are due to a different kind of radical formed by $\gamma$-irradiation of the crystal. Also, previous studies on the same system detected a second irradiation product present in an amount strongly dependent on the irradiation dose.[14]

**ENDOR.** The ENDOR spectra have been obtained in the frequency range 2−35 MHz, at 150 K, by saturating the central multiplet lines. The recorded ENDOR signals are due to the coupling with the protons of the radical(s). We will call high-frequency $\nu_+$ and low-frequency $\nu_-$ ENDOR transitions those given by $\nu_+ = |A/2| + \nu_H$ and $\nu_- = ||A/2| - \nu_H|$, respectively. $A$ is the hyperfine splitting and $\nu_H$ the free proton frequency.

Figure 4 shows the ENDOR spectra obtained with the magnetic field in the *ab* crystallographic plane at 30° (Figure 5a) and 72° (Figure 5b) from the axis *a*. In Figure 5, we report the angular dependencies of the ENDOR frequencies in the 18−35 MHz range obtained for the crystal rotations around the *a*, *b* and *c** axes, in sequence. Only the $\nu_+$ ENDOR frequencies that could be assigned are reported, along with the best fitted curves calculated by the usual first order analysis.[45] Figure 5 shows in the *bc** and *ab* planes a couple of curves deriving from the two magnetically nonequivalent crystal sites. Furthermore, an unusual feature is evident in the three planes: the ENDOR frequencies occur in closely matched pairs, yielding parallel fitting curves. This indicates that two slightly different tyrosyl radicals are formed in the crystal lattice. In fact, radicals giving rise to parallel ENDOR curves must have proton hyperfine tensors very similar to each other both for the size of the principal values and for the orientation of the principal axes in the crystal structure. This situation was not observed previously by Box and co-workers[29] in their ENDOR study on a $\gamma$-irradiated single crystal of L-Tyr HCl at 4.2 K.

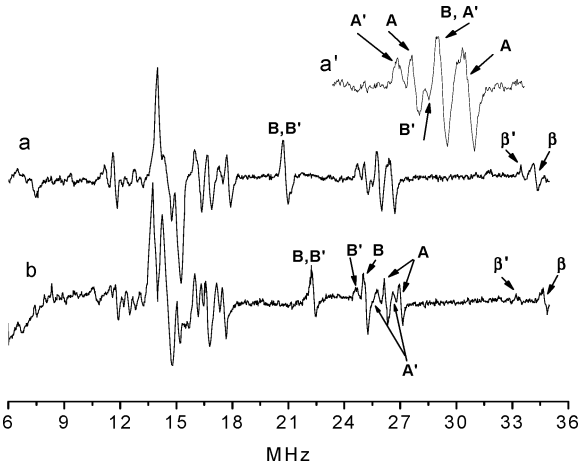


**Figure 4.** ENDOR spectra obtained with the magnetic field in the *ab* crystallographic plane at 30° (trace a) and 72° (trace b) from axis *a*. The spectra were obtained by saturating the central EPR line at the magnetic fields 340.45 mT (a) and 340.5 mT (b). The attribution of the signals to the tyrosyl radical protons is indicated. Trace a′ represents a magnification of spectrum a in the range 23−28 MHz.

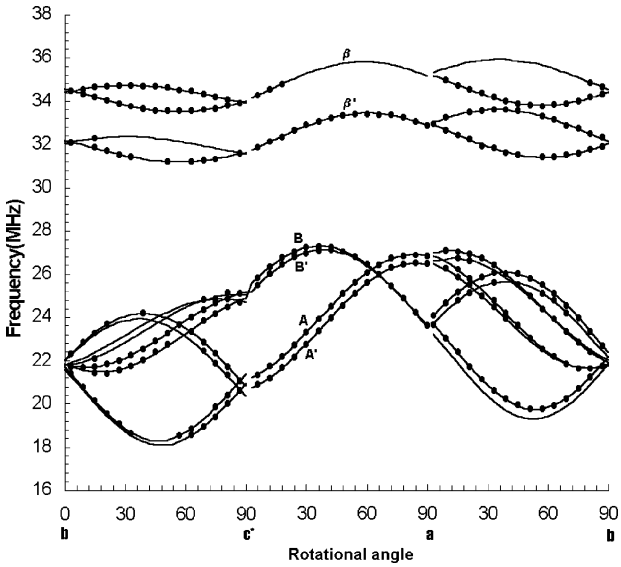


**Figure 5.** Angular dependencies of the ENDOR frequencies in the range 18−35 MHz obtained rotating the crystal around the *a*, *b* and *c** axes, in sequence. Only the $\nu_+$ ENDOR frequencies that could be assigned are reported, along with the best fitted curves calculated by the usual first order analysis.[45]

From the angular dependencies of the frequencies corresponding to the *A*, *A*′, *B* and *B*′ curves (see Figure 5), we have obtained the first four hyperfine tensors, reported in Table 1. Their dipolar principal values are typical of α-protons, and these can be identified with protons of the phenoxyl ring. Moreover, it is known[30,31] that H5 and H3 protons have hyperfine couplings much higher than H2 and H6 protons. The ENDOR lines of these latter protons should occur around the matrix proton frequency, in a region crowded with signals, and, in our case, this prevented a reliable determination of the corresponding hyperfine tensors.

A precise assignment of the *A*, *A*′, *B* and *B*′ tensors to the H3 and H5 protons of the two tyrosyl radicals can be done on the basis of the following analysis. It is well-known that the maximum dipolar value for an α-proton is approximately parallel to the C−H bond (namely, the *X*-direction), while the almost zero dipolar value is parallel to the lone electron p orbital (namely, the *Z*-direction).[45] The four proton tensors *A*, *A*′, *B* and *B*′ have about the same $T_{ZZ}$ principal direction (see Table 1), corresponding to the normal to the ring plane. Furthermore, by comparison with the neutron diffraction data,[48] we obtain that the tensors *A* and *A*′ have the $T_{XX}$ direction approximately parallel to the C3−H3 bond of the undamaged molecule, while for the *B* and *B*′ tensors the $T_{XX}$ direction is parallel to the C5−H5 bond of the same molecule. In Table 2, we report the angles between the principal directions of the four hyperfine tensors and the crystallographic directions corresponding to selected axes in the tyrosine molecule. From the previous considerations, we can attribute tensors *A* and *A*′ to the ring proton H5 and tensors *B* and *B*′ to the ring proton H3 in two slightly different tyrosyl radicals, hereafter indicated as PhO$^{\bullet}$ and PhO$^{\bullet\prime}$ radicals. (The assignment of the hyperfine tensors to protons of the same radical (PhO$^{\bullet}$ or PhO$^{\bullet\prime}$) has been done on the basis of the different intensity of the ENDOR lines: in fact, signals deriving from the coupling of *A*, *B* and *β* protons are always, irrespective of the saturated EPR line, more intense than signals from *A*′, *B*′ and *β*′ protons. As an example, the attribution of the ENDOR signals to the different protons is reported in Figure 4.)

Tensors *β* and *β*′ of Table 2 are typical of *β*-protons, for which axial dipolar tensors with small principal values are expected. Moreover, for *β*-protons, the principal axis corresponding to the largest dipolar value should be parallel to the $C_\alpha-H_\beta$ direction. From the comparison with neutron diffraction data,

**TABLE 1: Hyperfine Coupling Tensors of the Tyrosyl Radicals in Freshly γ-Irradiated Single Crystals of L-Tyr HCl**

| | | | | direction cosines | | |
|---|---|---|---|---|---|---|
| tensor[a] | principal values (MHz) | isotropic value (MHz) | dipolar principal values (MHz) | A | b | *c** |
| tensor *A*′ | −7.2 | | +9.5 | 0.0207 | −0.6337 | 0.7733 |
| (H3) | −18.2 | −16.7 | −1.5 | 0.3503 | −0.7198 | −0.5993 |
| | −24.8 | | −8.1 | 0.9364 | 0.2832 | 0.2071 |
| tensor *A* | −7.5 | | +9.8 | 0.0154 | −0.6634 | 0.7481 |
| (H3′) | −18.7 | −17.3 | −1.5 | 0.3410 | −0.6999 | −0.6276 |
| | −25.5 | | −8.3 | 0.9399 | 0.2647 | 0.2154 |
| tensor *B*′ | −6.9 | | +10.2 | 0.6379 | 0.6578 | −0.4004 |
| (H5) | −19.3 | −17.3 | −2.1 | 0.3497 | −0.7107 | −0.6104 |
| | −25.6 | | −8.3 | −0.6861 | 0.2494 | −0.6434 |
| tensor *B* | −7.9 | | +9.9 | 0.6452 | 0.6750 | −0.3579 |
| (H5′) | −19.1 | −17.8 | −1.3 | 0.3518 | −0.6783 | −0.6451 |
| | −26.4 | | −8.6 | −0.6782 | 0.2903 | −0.6751 |
| tensor *β* | 44.0 | | +3.9 | −0.7504 | −0.4884 | −0.4454 |
| (H7) | 38.7 | 40.1 | −1.4 | −0.4227 | 0.8726 | −0.2448 |
| | 37.6 | | −2.5 | 0.5082 | 0.0046 | −0.8612 |
| tensor *β*′ | 39.2 | | +3.9 | −0.7700 | −0.4869 | −0.4124 |
| (H7′) | 33.8 | 35.3 | −1.5 | −0.3978 | 0.8717 | −0.2863 |
| | 32.9 | | −2.4 | 0.4989 | −0.0564 | −0.8648 |

[a] For the *A*, *A*′, *B* and *B*′ tensors, the first line corresponds to the principal value $T_{XX}$ along the X-direction, while the second line corresponds to the principal value $T_{ZZ}$ along the Z-direction.

**TABLE 2: Orientation of the Principal Axes of Tensors *A* and *B* with respect to the Same Selected Directions in the Undamaged Molecule**

| directions[a] | angle | directions[a] | angle |
|---|---|---|---|
| $A_{XX}$,C5H5 | 7.9° | $B_{XX}$,C3H3 | 8.3° |
| $A_{ZZ}$,Pr | 3.0° | $B_{ZZ}$,Pr | 4.3° |
| $A_{YY}$,Prb5 | 7.6° | $B_{YY}$,Prb3 | 8.7° |
| $A_{XX}'$,C5H5 | 6.4° | $B_{XX}'$,C3H3 | 9.5° |
| $A_{ZZ}'$,Pr | 1.0° | $B_{ZZ}'$,Pr | 1.7° |
| $A_{YY}'$, Prb5 | 6.5° | $B_{YY}'$,Prb3 | 17.2° |

[a] Pr is the direction perpendicular to the ring, defined as the perpendicular to the C1C4 and C3C5 directions. Prb5 is the direction perpendicular to the Pr and C5H5 directions. Prb3 is the direction perpendicular to the Pr and C3H3 directions.

we found that the angle between this principal axis and the C1H7 direction of the undamaged molecule is 5.2 and 7.4° for the $\beta$ and $\beta'$ tensors, respectively, leading to the attribution of $\beta$ and $\beta'$ tensors to the H7 proton of the two PhO$^{\bullet}$ and PhO$^{\bullet\prime}$ radicals. The second $\beta$ proton (H8) of both tyrosyl radicals was not identified from the ENDOR frequencies. This can derive from the radical small hyperfine coupling, leading to ENDOR frequencies hidden in the crowded region near the free proton frequency $\nu_P$ (see the Supporting Information).

The well-known semiempirical expression[45]

$$A_{iso} = \rho_{\pi} B_2 \cos^2 \theta \qquad (1)$$

relates the isotropic coupling of $\beta$ protons to the unpaired spin density on the $C_\alpha$ carbon atom, $\rho_\pi$ and the dihedral angle defined by the methylene group carbon−proton bond and the normal to the phenyl ring, $\theta$. Therefore, the different h.c.c.s determined for the same $\beta$ proton of PhO$^{\bullet}$ and PhO$^{\bullet\prime}$ radicals can derive from (i) slightly different dihedral angles $\theta$ or from (ii) slightly different spin densities on the $C_\alpha$ carbon atom. This latter explanation is supported by the fact that the angular dependence of the hfc tensors of the $\beta$ protons is exactly the same in the three rotation planes, suggesting that both radicals have the same methylene conformation. In addition, also the H3 and H5 protons give each two sets of slightly different tensors. In particular, the difference in the isotropic couplings can only derive from a different spin density on the carbon atom attached to the considered proton. All of these considerations support the idea of the presence of two tyrosyl radicals with slightly different spin density maps.

**High-Frequency EPR.** The HF-EPR spectra have been recorded at different times after the crystal irradiation. They evidence that changes occur in the structure of the formed radical species upon crystal aging.

The spectra of powdered fresh samples were obtained at different mw frequencies (about 220 and 330 GHz). Spectra of aged (about 1 year old) samples were obtained at about 330 GHz. The spectra of fresh and aged samples, both recorded at 325.55 GHz, are shown in Figure 6, traces a, panels 1 and 2, respectively (spectra of fresh crystals at 220 GHz are shown in the Supporting Information). The spectra are dominated by the $g$ tensor anisotropy of the tyrosyl radical(s) and show at low field a well-defined feature corresponding to the maximum principal component $g_{xx}$. This feature undergoes a clear shift to lower fields upon crystal aging (compare spectra in Figure 6, panels 1 and 2). This shift is accompanied by a reduction of the hyperfine structure, producing a minor total line width. For the fresh sample, the line width in the $g_{xx}$ component is about 40 G at 330 GHz (reduced to 32 G at 220 GHz, see Supporting Information), while it is 26 G for the aged sample. Differences between fresh and aged samples are also evident in the high-field part of the spectra. At these field positions, the total spectral intensity derives from the superposition of the tyrosyl radical-(s) signal (corresponding to the $g_{yy}$ and $g_{zz}$ components) with the signal due to different radical(s). All of the above spectral modifications point to a change, with aging, of the structure and/or orientation in the crystal lattice of the radicals initially formed.

We start the analysis from the spectrum of the aged sample, where the $g_{xx}$ feature shows a clear splitting in five hyperfine components, pointing to the presence of only one tyrosyl radical.[5] The spectrum of this radical has been simulated by taking into account the hyperfine tensors obtained for the tyrosyl radical of the fresh sample (Table 1). (As already stated, ENDOR analysis, necessary in order to obtain the hyperfine coupling tensors, was performed only on freshly irradiated crystals and not on aged crystals because of practical reasons. However, as simulations clearly show, convincing analysis can be obtained starting from the hfc tensors of fresh samples, and slightly adjusting their principal values.) H(3) and H(5) protons were considered as equivalent, and their hyperfine principal values were taken as the average of the corresponding principal values of the four hyperfine tensors $A$, $A'$, $B$ and $B'$ of Table 1. An isotropic coupling of 4 MHz was used for H(2) and H(6) protons, whose hyperfine tensors were not determined from ENDOR spectra. Only one $\beta$ proton was considered in the simulation. To obtain convincing simulations, it was necessary to use, for this proton, hyperfine tensor components slightly higher than those obtained for the $\beta$ and $\beta'$ protons in fresh samples. The simulated spectrum is shown in Figure 6 (panel 2, trace c), and the parameters used for the simulation are reported in Table 3. It is evident that a second radical species contributes to the experimental spectrum at field positions higher than that corresponding to the $g_{yy}$ component of the tyrosyl radical.

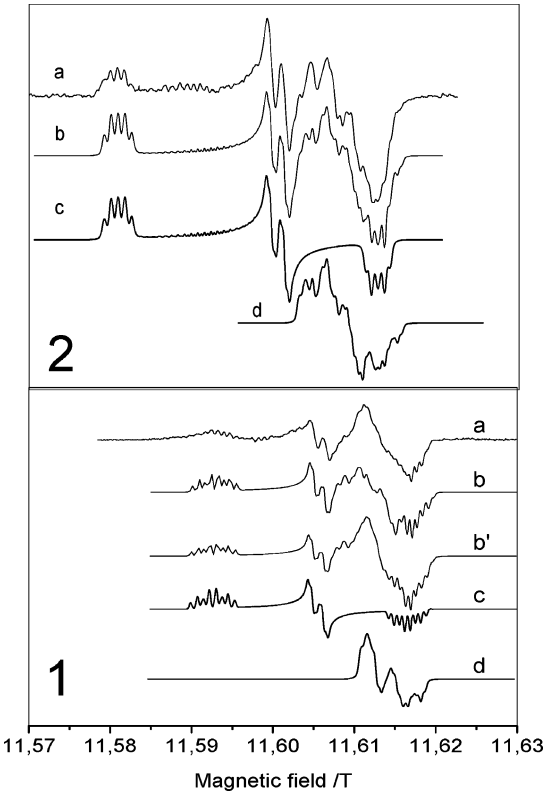


**Figure 6.** Powder EPR spectra at 325.55 GHz of fresh (panel 1, $T$ = 70 K) and aged (panel 2, $T$ = 25 K) samples of L-Tyr HCl. Panel 1: trace a, experimental spectrum; traces b−d, calculated spectra. Panel 2: trace a, experimental spectrum; traces b−d, calculated spectra. Spectrum b in panel 1 is obtained by summing spectrum c in panel 1 and spectrum d of panel 2 (see text for details). Spectrum b′ in panel 1 is obtained by summing spectrum c in panel 1 and spectra d in panels 1 and 2 (see text for details). Spectrum b is obtained by summing spectrum c and spectrum d (see text for details).

In a previous work on radicals produced by $\gamma$-irradiation in *N*-acetyl-L-tyrosine single crystals,[31] we were able to obtain a complete set of proton hyperfine tensors of a second radical (besides the tyrosyl radical), that was identified as the product of hydrogen addition to the phenolic ring (cyclohexadienylic radical, hereafter indicated by Chd$^{\bullet}$). This radical was supposed to be formed by $\gamma$-irradiation also in L-Tyr HCl powders.[14] On this ground, the spectrum obtained as the difference between the experimental and calculated tyrosyl spectra was simulated

**TABLE 3: *g* and Proton Hyperfine Coupling Tensors[a] of the Tyrosyl Radicals as Obtained from the Simulation of the HF-EPR Spectra and from the X-Band ENDOR Data**

| | PhO• | PhO•′ | PhO•″ |
|---|---|---|---|
| $g_{xx}$ | 2.00661 | 2.00621 | 2.00769 |
| $g_{yy}$ | 2.00418 | 2.00418 | 2.00430 |
| $g_{zz}$ | 2.00244 | 2.00212 | 2.00218 |
| $H_{3,5}$[b] $A_{XX}$ | −23 | −23 | −23 |
| $A_{YY}$ | −10.5 | −10.5 | −10.5 |
| $A_{ZZ}$ | −19 | −19 | −19 |
| $A_{XY}$ | 6.5 | 6.5 | 6.5 |
| $H_{2,6}$ $A_{XX}$ | 4 | 4 | 4 |
| $A_{YY}$ | 4 | 4 | 4 |
| $A_{ZZ}$ | 4 | 4 | 4 |
| $A_{XY}$ | 0 | 0 | 0 |
| $H_{\beta}$ $A_{XX}$ | 44 | 39.2 | 47 |
| $A_{YY}$ | 38.7 | 33.8 | 45 |
| $A_{ZZ}$ | 37.6 | 32.9 | 45 |
| $A_{XY}$ | 0 | 0 | 0 |

[a] Hyperfine couplings in MHz. [b] The hyperfine couplings of ring protons were calculated by rotating the experimental hyperfine tensors (from ENDOR data) into the *g* tensor principal system; the undamaged tyrosine molecule and the tyrosyl radicals were assumed to have the same orientation in the crystal lattice.

by assuming the presence of a Chd• radical. The simulation reported in panel 2, trace d, has been obtained by using the *g* tensor principal components: $g_{xx}$(Chd•) = 2.00355, $g_{yy}$(Chd•) = 2.00315, $g_{zz}$(Chd•) = 2.00250, and for the proton hyperfine tensors those determined for the Chd• radical in *N*-acetyl-L-tyrosine single crystals.[31] The very good accord between the experimental spectrum and simulation (panel 2, trace b) obtained by summing the calculated spectra of tyrosyl and Chd• radicals confirms the presence of both radicals in aged samples of $\gamma$-irradiated L-Tyr HCl crystals.

The previous discussion has shown that the 300 GHz EPR spectrum of the aged sample is consistent with the presence, in high amount, of only one tyrosyl radical, with $g_{xx}$ = 2.00769. This radical (hereafter referred to as PhO•″) differs from PhO• and PhO•′ radicals at least for the hyperfine coupling of the $\beta$ proton and for the *g* tensor components (see below). (It has to be noted that, in the spectrum of Figure 6, panel 2, trace a, weak features are visible at field positions between the $g_{xx}$ and $g_{yy}$ components of the PhO•″ radical. These features compare well to the low-field spectral component in the spectrum of the fresh sample (Figure 6, trace a): it is evident that PhO• and PhO•′ radicals evolve to a third radical PhO•″, but in the old sample, a little amount of the initial radicals is still present.)

In the following, we discuss the spectra of the fresh sample: the ENDOR results show the presence of two tyrosyl radicals having slightly different spin density distributions. In the HF spectra, the low-field component of the fresh sample is broader and more structured than that in the aged sample. This strongly supports that PhO• and PhO•′ radicals have also different $g_{xx}$ components. The HF-EPR spectra of fresh samples were simulated as the superposition of signals from the PhO• and PhO•′ radicals with slightly different *g* tensors (the hfc tensors were taken from ENDOR results) (see trace c in panel 1 of Figure 6). The HF-EPR powder spectrum is not sensitive to the slight difference in the hfc tensors of the ring protons between the PhO• and PhO•′ radicals. For this reason, in the simulations, only the $\beta$ proton couplings have been taken different for the two tyrosyl radicals. The parameters used in the reported simulation are summarized in Table 3. Regarding the *g* tensors, the two radicals differ mainly for the $g_{xx}$ component, while $g_{yy}$ appears to be the same, as evident from the well-defined central region of the spectrum consisting of a doublet that derives mainly from the coupling of the $\beta$ proton along the $g_{yy}$ principal direction. Assuming sligthly different $g_{zz}$ components, it was possible to reproduce the hyperfine structure evident at high fields. (Because of the presence, at high fields, of the signal of the Chd• radical, the $g_{zz}$ values are determined with an error slightly higher than the $g_{xx}$ and $g_{yy}$ components.) The spectrum of the fresh sample recorded at 220 GHz has been simulated with the same parameters used for the 330 GHz simulation: experimental and simulated spectra are shown in Figure 1S of the Supporting Information. It has to be noted that the calculated tyrosyl spectra reproduces fairly well the low-field feature, both at 220 and 330 GHz. The difference in the total line width of the $g_{xx}$ component at the two microwave frequencies (about 8 G) is consistent with the reduction expected on the basis of the $g_{xx}$ difference ($\Delta$ = 0.0004) between the two radicals.

If we add the spectrum calculated for the Chd• radical (spectrum d in panel 2 of Figure 6) to the calculated spectra of PhO• and PhO•′, the resulting spectrum (trace b in panel 1 of Figure 6) does not reproduce perfectly the central part of the fresh sample spectrum, probably because of the presence of a small concentration of further radical species. We have speculated that also Chd• radical can be present in two different conformations, with slightly different hyperfine tensors of the $\beta$ protons. The calculated spectrum of this second Chd• radical is shown as trace d in panel 1. With this assumption, we have obtained a total calculated spectrum that reasonably reproduces the experimental spectra at both ~330 and ~220 GHz (see the Supporting Information.). However, the presence of two Chd• radicals should be considered a speculation, in the absence of further experimental support.

## Discussion

**Magnetic Parameters and Role of H-Bonding.** The data analysis has shown that both reduction and oxidation products are formed by $\gamma$-irradiation in L-Tyr HCl crystals. In particular, two slightly different tyrosyl radicals (oxidation products) are formed in fresh samples. They have the same electronic structure and occupy the same position in the crystal lattice. The difference in their magnetic parameters, *g* and hfc tensors, is very small when compared to differences among tyrosyl radicals in different biological systems existing in the literature.[15] Thus, it is quite logical to suppose that the effect at the origin of this difference is also small.

From the crystal structure of L-Tyr HCl, the phenolic oxygen of the tyrosine molecule is involved as an acceptor in a hydrogen bond with a COOH group; the distance between the O of the tyrosine molecule and the H of the COOH group is 1.609 Å.[48] Because the two tyrosyl radicals occupy the same lattice position of the undamaged molecule (see the Results section), both of them have the phenoxyl oxygen involved in a H-bond interaction with COOH. Several works have shown that in tyrosyl radicals the presence of a H-bond on the phenoxyl oxygen lowers the $g_{xx}$ value and that the stronger the H-bond, the lower the $g_{xx}$ value.[40,44] Then, a difference in the H-bonding status between the two tyrosyl radicals is able to explain directly their different $g_{xx}$ parameters; in particular, it is possible that the radical with the lower $g_{xx}$ value could have its phenoxyl oxygen involved in more than one hydrogen bond. In principle, differences in $g_{xx}$ could also derive from differences in the polarity of the radical environment.[40] However, in our case, $\gamma$-irradiation creates a limited amount of radicals, without altering the surrounding crystal structure

A H-bonding interaction involving the phenoxyl oxygen as an acceptor is believed to modify also the spin density map of

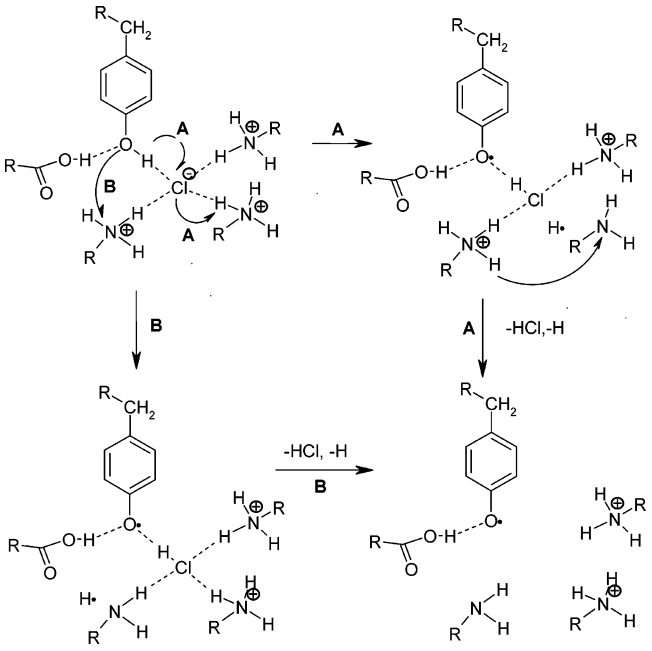


**Figure 7.** Proposed mechanisms for the formation of the tyrosyl radicals: (A) Route A involves initial hydrogen atom transfer from TyrOH to $Cl^-$ and $Cl^-$ gives an electron to one of the three amine protons H-bonded to it; (B) route B involves a proton transfer from TyrOH to $Cl^-$, while the electron migrates to a close $RNH_3^+$ group.

the radical,[25] and theoretical calculations have been performed in order to quantify and rationalize this effect (refs 41, 46, 57 and 58 and references therein). The presence of a H-bond would lower the absolute value of the ring proton hyperfine couplings,[57] and this is what we observe for H3 and H5 protons of $PhO^•$ and $PhO^{•\prime}$ (see Table 2). Therefore, a different H-bonding status could account for all of the differences in the magnetic parameters of the two radicals.

It is also important to point out that the $g_{xx}$ value we measured for $PhO^{•\prime}$, to our knowledge, is the lowest ever reported in the literature for tyrosyl radicals. It is worth mentioning that a slightly higher $g_{xx}$ value (2.00645) has been reported for the so-called $TyrD^•$ radical in photosystem II,[59] a radical that is strongly hydrogen-bonded to a nearby histidine.

**Molecular Scenario.** In this section, we propose a molecular scenario that can explain the presence of two different tyrosyl radicals with low (2.00661) and very low (2.00621) $g_{xx}$ values, and the slow evolution of these two radicals to give a third tyrosyl radical with a relatively high $g_{xx}$ value (2.00769). To rationalize our results, we have focused our attention on the network of H-bonds present in the undamaged L-Tyr HCl crystal, where five hydrogen bonds are located in the immediate surroundings of the phenolic OH group. This is directly involved in two H-bonds: one as an acceptor (the donor being the COOH moiety of a neighboring tyrosine molecule) and one as a donor (the acceptor being the chloride ion). The phenoxyl radical is obtained by the homolytic cleavage of the phenolic OH bond, with hydrogen loss. In L-Tyr HCl crystals, we propose two possible, more complex mechanisms, reflecting the peculiar microenvironment of the tyrosine phenol group.

Figure 7 can help clarify the models we are proposing. The first possibility (route A) is that, under the effect of $\gamma$-irradiation, an H atom is transferred to $Cl^-$, which in turn gives an electron to one of the three amine protons H-bonded to it. The process leading to the formation of the phenoxyl radical could be seen as a hydrogen atom transfer (HAT), with the overall reaction $PhOH + Cl^- + RNH_3^+ \rightarrow PhO^• + HCl + H^• + RNH_2$ (see Figure 7). We think that this mechanism could be made possible by the complex hydrogen-bond network existing in the L-Tyr HCl crystal structure. The hydrogen atom can either recombine with another $H^•$ to produce $H_2$ or attack the phenolic ring of another tyrosine molecule (not necessarily a neighboring one) to give the observed cyclohexadyenilic radical.

A second possibility (route B) is that, under the effect of $\gamma$-irradiation, an electron leaves the phenol ring and simultaneously a proton is transferred to the $Cl^-$ anion to give HCl. The leaving electron is captured by a $-NH_3^+$ group (possibly one of the three $-NH_3^+$ H-bonded to the $Cl^-$ anion that is accepting the proton). The overall reaction is the same as before ($PhOH + Cl^- + RNH_3^+ \rightarrow PhO^• + HCl + H^• + RNH_2$), but the mechanism is different. In this case, the process that produces the phenoxyl radical could be seen as a proton-coupled electron transfer (PCET).

Whatever the mechanism, in both cases, a HCl molecule is formed: this molecule is trapped in the lattice and involved, as a donor, in a hydrogen bond with the phenoxyl oxygen of the newly created radical. In the undamaged crystal, the phenolic oxygen is H-bonded, as an acceptor, with a nearby COOH and the phenoxyl oxygen retains this H-bond in the irradiated crystal (see the Results section). Therefore, the phenoxyl radical is involved, as an acceptor, in two hydrogen bonds (the donors being COOH and HCl). It is important to point out that the formed HCl molecule is "trapped" in the crystal lattice by the presence of several hydrogen bonds, so its escape is hampered.

The proposed models qualitatively explain quite well the observed results. The two radicals with low (2.00661) and very low (2.00621) $g_{xx}$ values could correspond to two different global arrangements of the above-mentioned scenario (with a network of several hydrogen bonds, it is quite logical that more than a single energy minimum exists).

The very slow conversion into the third species (with $g_{xx} = 2.00769$) would be explained by the slow escape of the HCl molecule as a gas, leaving behind a situation where the phenoxyl oxygen is involved in just one hydrogen bond with the COOH group.

To support our interpretation, we performed DFT calculations on simplified molecular models picturing the situation exposed in our scenario (for a discussion of the model, see the Experimental Methods section, paragraph Computational Details). DFT calculation of the $g$ tensor for the model system containing the HCl molecule (Figure 1b) gave $g_{xx} = 2.00645$, $g_{yy} = 2.00437$ and $g_{zz} = 2.00226$. Although the model we used in the calculation is clearly rough, we obtained a very good match between the calculated tensor and the $g$ tensors of $PhO^•$ and $PhO^{•\prime}$ radicals. In particular, the calculated $g_{xx}$ is in between the $g_{xx}$ values of $PhO^•$ and $PhO^{•\prime}$, suggesting that these radicals are bound both to the COOH group and to HCl, but the overall H-bond strength is slightly different for the two radicals, probably because of small changes in the HCl position.

Performing the same calculation for the model system without HCl, we obtained $g_{xx} = 2.00775$, $g_{yy} = 2.00451$ and $g_{zz} = 2.00219$. A very good match exists between the calculated $g$ tensor and the $g$ tensor of the $PhO^{•\prime\prime}$ radical, supporting our hypothesis of the escape of the HCl molecule. Experimental and calculated $g$ tensors are summarized in Table 4.

**H-Bonding and Tyrosine Redox Chemistry.** The coupling between electron and proton transfer reaction upon tyrosine oxidation and tyrosyl radical reduction is believed to regulate the biological role of the tyrosine/tyrosyl radical couple.[15,18] Such an effect seems to be particularly crucial in the mechanism of photoinduced water splitting in photosystem II (PS II) from

**TABLE 4: Comparison between Experimental and Calculated *g* Tensors of the Tyrosyl Radicals**

| | PhO•[a] | PhO•′[a] | PhO•″[a] | calcd[b] | calcd[c] |
|---|---|---|---|---|---|
| $g_{xx}$ | 2.00621 | 2.00661 | 2.00769 | 2.00775 | 2.00645 |
| $g_{yy}$ | 2.00418 | 2.00418 | 2.00430 | 2.00451 | 2.00437 |
| $g_{zz}$ | 2.00212 | 2.00244 | 2.00218 | 2.00219 | 2.00226 |

[a] Experimental (estimated error ±0.00002). [b] Calculated (DFT-B3LYP, 6-31+G(d,p)) without HCl (see text). [c] Calculated (DFT-B3LYP, 6-31+G(d,p)) with HCl (see text).

plants and cyanobacteria (refs 60−62 and references therein). In fact, the oxidation of the so-called tyrosine Z (tyrZ) residue by the primary donor $P_{680}$ is coupled to the proton transfer from tyrosine to a nearby H-bonded histidine. Indeed, there are marked similarities between the tyrZ oxidation in PSII and the mechanisms proposed for the phenol ring oxidation taking place in L-Tyr HCl crystals. The two mechanisms involve either (1) a hydrogen atom transfer to a nearby $Cl^-$ ion, previously H-bonded to the phenolic OH group, or (2) a proton-coupled electron transfer in which the proton transfer from the phenolic OH to the H-bonded $Cl^-$ is coupled to an electron transfer in the crystal. As in the case of tyrosine oxidation in PSII, there is a hydrogen bond which provides a path for proton transfer, after which a reversed hydrogen-bond interaction is established (the acceptor becomes a donor and vice versa).

Another interesting similarity between the tyrosyl radicals in PSII and L-Tyr HCl crystals concerns the process of radical reduction. It has been proposed that the reduction of the tyrosyl radical (tyrZ•) takes place through a hydrogen atom transfer from the manganese cluster.[62] A previous EPR investigation[32] on radicals formed in L-Tyr HCl single crystals reported the disappearance of the tyrosyl radical upon exposure of the irradiated crystal to light with $\lambda > 310$ nm and the formation of a new radical species, identified as a decarboxylation product. From literature data, it is known that light absorption induces a strong increase in the capability of phenoxyl radicals in extracting a hydrogen atom.[63,64] We know that in L-Tyr HCl crystals the OH of the COOH group is H-bonded to the phenoxyl oxygen.[48] Then, a reasonable mechanism for the formation of the carbon-centered radical reported in ref 32 can involve (i) H atom extraction from COOH by the excited phenoxyl radical and (ii) formation (and escape) of a $CO_2$ molecule resulting in the decarboxylation radical. Decarboxylation is a general mechanism observed in irradiated amino acids, even though normally it does not seem to be efficient in the case of aromatic amino acids.[65] On the basis of this mechanism, the light-induced reduction of the phenoxyl radical in L-Tyr HCl would take place through a hydrogen atom transfer from a neighboring molecule, like the mechanism proposed in PSII.

In conclusion, the proposed mechanisms underlying the formation of the observed tyrosyl radicals in L-Tyr HCl crystals are strongly influenced by the presence of a complex network of hydrogen-bond interactions, which favor directional hydrogen atom transfer and/or directional proton-coupled electron transfer reactions both in phenol oxidation (this work) and in phenoxyl reduction (the investigation carried out by Pasoyan et al.[32]). These kinds of interactions seems to be crucial in regulating radiation chemistry in organic solids, as well as in regulating redox chemistry in proteins.

**Acknowledgment.** We thank the NHMFL of Tallahassee, FL, for the use of the HF-EMR facility. We thank Dr. Sun Un and Prof. Einar Sagstuen for helpful discussion. V.C. acknowledges financial support from the Italian National Research Council under the CNR-NATO Outreach Fellowships program.

**Supporting Information Available:** Full list of authors of ref 51; a short discussion about the isotropic coupling constants of $\beta$ protons; the experimental spectrum of the fresh sample at 210.5 GHz, together with the simulation. This material is available free of charge via the Internet at http://pubs.acs.org.

## References and Notes

(1) Pedersen, J. Z.; Finazzi-Agro, A. *FEBS Lett.* **1993**, *325*, 53−58.
(2) Stubbe, J.; van der Donk, W. A. *Chem. Rev.* **1998**, *98*, 705−762.
(3) Reece, S. Y.; Hodgkiss, J M.; Stubbe, J.; Nocera, D. G. *Philos. Trans. R. Soc. London, Ser. B* **2006**, *361*, 1351−1364.
(4) Stubbe, J. *Chem. Commun.* **2003**, *20*, 2511−2513.
(5) Lendzian, F. *Biochim. Biophys. Acta* **2005**, *1707*, 67−90.
(6) Tsai, A.; Kulmacz, R. J. *Prostaglandins Other Lipid Mediators* **2000**, *62*, 231−254.
(7) Pujols-Ayala, I.; Barry, B. A. *Biochim. Biophys. Acta* **2004**, *1655*, 205−216.
(8) Ivancich, A.; Jouve, H. M.; Gaillard, J. *J. Am. Chem. Soc.* **1996**, *118*, 12852−12853.
(9) Chouchane, S.; Girotto, S.; Yu, S.; Magliozzo, R. S. *J. Biol. Chem.* **2002**, *277*, 42633−42638.
(10) Ivancich, A.; Jakopitsch, C.; Aur, M.; Un, S.; Obinger, C. *J. Am. Chem. Soc.* **2003**, *125*, 14093−14102.
(11) Su, C.; Shalin, M.; Oliw, E. W. *J. Biol. Chem.* **1998**, *273*, 20744−20751.
(12) Ivancich, A.; Mazza, G.; Desbois, A. *Biochemistry* **2001**, *40*, 6860−6866.
(13) Schunemann, V.; Jung, C.; Trautwein, A. X.; Mandon, D.; Weiss, R. *FEBS Lett.* **2000**, *179*, 149−154.
(14) Ivancich, A.; Dorlet, P.; Goodin, D. B.; Un, S. *J. Am. Chem. Soc.* **2001**, *123*, 5050−5058.
(15) Pesavento, R. P.; Van Der Donk, W A. *Adv. Protein Chem.* **2001**, *58*, 317−385.
(16) Rogers, M. S.; Dooley, D. M. *Curr. Opin. Chem. Biol.* **2003**, *7*, 189−196.
(17) Stubbe, J. *Curr. Opin. Chem. Biol.* **2003**, *7*, 183−188.
(18) Hoganson, C. W.; Tommos, C. *Biochim. Biophys. Acta* **2004**, *1655*, 116−122.
(19) Heinecke, J. W. *Toxicology* **2002**, *177*, 11−22.
(20) Heinecke J. W. *Am. J. Cardiol.* **2003**, *91* (3A), 12A−16A.
(21) Barnham, K. J.; Haeffner, F.; Ciccotosto, G. D.; Curtain, C. C.; Tew, D.; Mavros, C.; Beyreuther, K.; Carrington, D.; Masters, C. L.; Cherny, R. A.; Cappai, R.; Bush, A. I. *FASEB J.* **2004**, *18*, 1427−1429.
(22) Murakami, K.; Irie, K.; Ohigashi, H.; Hara, H.; Nagao, M.; Shimizu, T.; Shirasawa, T. *J. Am. Chem. Soc.* **2005**, *127*, 15168−15174.
(23) Kochman, A.; Koska, Cz.; Metodiewa, D. *Amino Acids* **2002**, *23*, 95−101.
(24) Jeschke, G. *Biochim. Biophys. Acta* **2005**, *1707*, 91−102.
(25) Lucarini, M.; Mugnaini, V.; Pedulli, G. F.; Guerra, M. *J. Am. Chem. Soc.* **2003**, *125*, 8318−8329.
(26) Maki, T.; Araki, Y.; Ishida, Y.; Onomura, O.; Matsumura, Y. *J. Am. Chem. Soc.* **2001**, *123*, 3371−3372.
(27) Barry, B.; Einarsdottir, O. *J. Phys. Chem. B* **2005**, *109*, 6972−6981.
(28) Westerlund, K.; Berry, B. W.; Privett, H. K.; Tommos, C. *Biochim. Biophys. Acta* **2005**, *1707*, 103−116.
(29) Box, H. C.; Budzinski, E. E.; Freund, H. G. *J. Chem. Phys.* **1974**, *61*, 2222−2226.
(30) Fasanella, E L.; Gordy, W. *Proc. Natl. Acad. Sci. U.S.A.* **1969**, *62*, 299−304.
(31) Mezzetti, A.; Maniero, A. L.; Brustolon, M.; Giacometti, G.; Brunel, L. C. *J. Phys. Chem. A* **1999**, *103*, 9636−9643.
(32) Pasoyan, V. G.; Pulatova, M. K.; Kayushin, L. P. *Biofizika* **1972**, *17*, 1007−1011.
(33) Pasoyan, V. G.; Pulatova, M. K.; Kayushin, L. P. *Biofizika* **1970**, *15*, 12−19.
(34) Clancy, C. M. R.; Forbes, M. D. E. *Photochem. Photobiol.* **1999**, *69*, 16−21.
(35) Sealy, R. C.; Harman, L; West, P. R.; Mason, R. P. *J. Am. Chem. Soc.* **1985**, *107*, 3401−3406.
(36) Tomkiewicz, M.; McAlpine, R. D.; Cocivera, M. *Can. J. Chem.* **1972**, *50*, 3849−3856.
(37) Hulsebosch, R. J.; van den Brink, J. S.; Nieuwenhuis, S. A. M.; Gast, P.; Raap, J.; Lugtenburg, J.; Hoff, A. J. *J. Am. Chem. Soc.* **1997**, *119*, 8685−8694.
(38) Berthomieu, C.; Boussac, A. *Biospectroscopy* **1995**, *1*, 187−206.
(39) Warncke, K.; Perry, M. S. *Biochim. Biophys. Acta* **2001**, *1545*, 1−5.
(40) Un, S. *Magn. Reson. Chem.* **2005**, *43*, S229−S236.
(41) Wu, P.; O'Malley, P. J. *THEOCHEM* **2005**, *730*, 251−254.
(42) Langella, E.; Improta, R.; Barone, V. *J. Am. Chem. Soc.* **2002**, *124*, 11531−11540.

(43) Engstroem, M.; Himo, F.; Graeslund, A.; Minaev, B.; Vahtras, O.; Agren, H. *J. Phys. Chem. A* **2000**, *104*, 5149−5153.
(44) Un, S.; Atta, M.; Fontecave, M.; Rutherford, A. W. *J. Am. Chem. Soc.* **1995**, *117*, 10713−10719.
(45) Atherton, N. M. *Electron Spin Resonance*; Ellis Horwood: London, 1973.
(46) Farrar, C. T.; Gerfen, G. J.; Griffin, R. G.; Force, D. A.; Britt, R. D. *J. Phys. Chem. B* **1997**, *101*, 6634−6641.
(47) Koszelak, S. N.; Van der Helm, D. *Acta Crystallogr., Sect. B* **1981**, *B37*, 1122−1124.
(48) Frey, M. N.; Koetzle, T. F.; Koetzle, F.; Lehmann, M. S.; Hamilton, W. C. *J. Chem. Phys.* **1973**, *58*, 2547−2556.
(49) Srinivasan R. *Proc. Indian Acad. Sci.* **1959**, *A50*, 19−50.
(50) Hassan, A. K.; Pardi, L. A.; Krzystek, J.; Sienkiewicz, A.; Goy, P.; Rohrer, M.; Brunel, L. C. *J. Magn. Reson.* **2000**, *142*, 300−312.
(51) Frisch, M. J.; et al. *Gaussian 03*, revision C.02; Gaussian, Inc.: Wallingford, CT, 2004.
(52) Stewart, J. J. P. *J. Comput. Chem.* **1989**, *10*, 209−220.
(53) Becke, A. D. *J. Chem. Phys.* **1993**, *98*, 5648−5652.
(54) Lee, C.; Yang, W.; Parr, R. G. *Phys. Rev. B* **1988**, *37*, 785−789.
(55) Ditchfield, R.; Hehre, W. J.; Pople, J. A. *J. Chem. Phys.* **1971**, *54*, 724−728.
(56) Ruud, K.; Helgaker, T.; Bak, K. L.; Jørgensen, P.; Jensen, H. J. A. *J. Chem. Phys.* **1993**, *99*, 3847−3859.
(57) O'Malley, P. J.; Ellson, D. *Biochim. Biophys. Acta* **1997**, *1320*, 65−72.
(58) Himo, F.; Graslund, A.; Eriksson, L. A. *Biophys. J.* **1997**, *72*, 1556−1567.
(59) Faller, P.; Goussias, C.; Rutherford, A. W.; Un, S. *Proc. Natl. Acad. Sci. U.S.A.* **2003**, *100*, 8732−8735.
(60) Barber, J. *Biochim. Biophys. Acta* **2004**, *1655*, 123−132.
(61) Diner, B. A. *Biochim. Biophys. Acta* **2001**, *1503*, 147−163.
(62) Tommos, C.; Babcock, G. T. *Biochim. Biophys. Acta* **2000**, *1458*, 199−219.
(63) Kuzmin, V. A.; Khudjakov, I. V.; Tatikolov, A. S. *Chem. Phys. Lett.* **1977**, *49*, 495−497.
(64) Ganyuk, L. N.; Melezhik, A. V.; Pokhodenko, V. D. *Dopov. Akad. Nauk B* **1976**, *5*, 423−426.
(65) Box, H. C. *Radiation Effects: ESR and ENDOR Analysis*; Academic Press: New York, 1977.